J Electroceram (2009) 23:478–483
DOI 10.1007/s10832-008-9500-8

Fabrication of a superconducting flux flow transistor with a serial-channel structure by an AFM lithography method

Seokcheol Ko · Seong-Jong Kim · Byoung-Sung Han

Received: 19 May 2007 / Accepted: 2 April 2008 / Published online: 29 April 2008

Abstract Atomic force microscopy (AFM) has become an attractive technique to fabricate nano devices since the observing mechanism is different from fabricating one. We have fabricated the superconducting flux flow transistor (SFFT) with a serial-channel structure using the AFM lithography analyzed the modified surface by the AFM image. We investigated the induced voltage in a serial-channel terminals dependence on the gate current by the *I–V* measurement system. We performed the numerical simulation to get the theoretical characteristics of the SFFT controlled by the gate current via the modified channel. The transresistance was 0.006 Ω for I_d=51 mA at I_g=5 mA. It is very low transresistance in comparison with SFFTs fabricated by the other processes, however our results show that the SFFT with a serial-channel structure is effectively fabricated by an AFM lithography method.

Keywords SFFT · AFM lithography · Serial-channel · Transresistance

S. Ko (✉)
Jeonnam Regional Innovation Agency,
1000 Namak-Ri, Samhyang-Myun,
Muan-Gun, Jeonnam 534-700, South Korea
e-mail: suntrac@jina.re.kr

S.-J. Kim
Mokpo Maritime University,
Chukkyo-Dong,
Mokpo City, Jeonnam 530-729, South Korea

B.-S. Han
Division of Electronics and Information Engineering,
Chonbuk National University,
664-14 Dukjin-Dong 1Ga,
Jeonju 561-756, South Korea

1 Introduction

The first report of tip-induced oxidation of silicon was a scanning tunneling microscope (STM) study by Dagata et al. [1]. They have showed the possibility of creating an oxide pattern with nanometric dimensions on a H-passivated surface with a STM operating in air, other groups have worked on the oxidation of silicon surfaces using an atomic force microscope (AFM) with a conducting probe in contact [2–4] and noncontact modes [5, 6]. AFM has become an attractive technique to fabricate nano devices since the observing mechanism is different from fabricating one. So far, method using AFM lithography was used to structure various materials like metals [7], polymer films [8], combined polymer metal resists [9], semiconductor surfaces [10], GaAs/AlGaAs heterostructures [11], and Nb or NbN ultrathin film [12]. Recently, AFM tip-induced oxide lines have been used as etching masks to demonstrate a Si metal-oxide-semiconductor field-effect transistor (MOSFET) [13], side-gate FET [14], organic thin-film field-effect transistor [15] and diamond single-hole transistors [16]. On a superconducting thin film, Song et al. [17] have reported that the surface modification of $YBa_2Cu_3O_{7-\delta}$ (YBCO) strips in the field of AFM tip leads to the controlled and systematic growth of protrusions across the entire strip. Although fabrication of electronic devices using an AFM tip-induced oxidation process has been studied by several authors in the case of Si [13] and Ti [18], it has been studied little for YBCO. So we have tried to fabricate a variety of superconducting flux flow transistors (SFFTs) [19–23] using an AFM lithography method.

In this paper, we fabricated the serial-channel SFFT using the selective anodization process induced by an AFM bias voltage tip. We analyze the modified surface by the

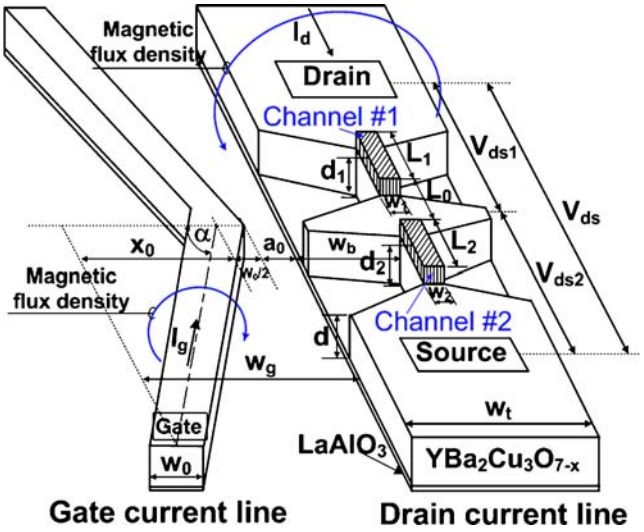

Fig. 1 A scheme of a serial-channel SFFT

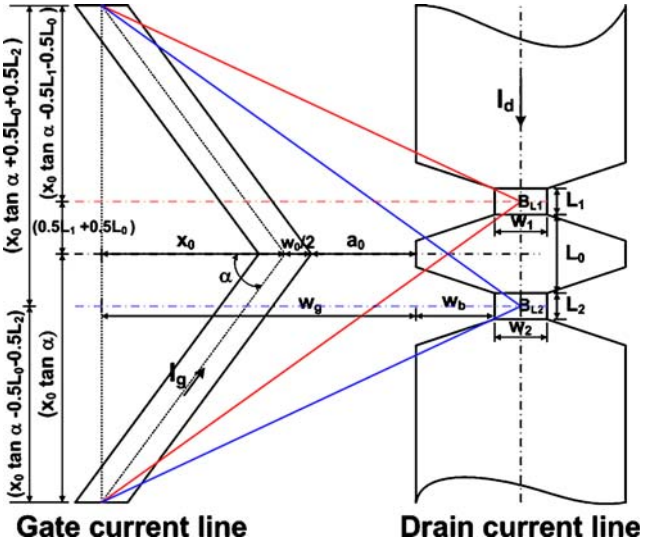

Fig. 2 Magnetic density calculation for a serial-channel SFFT when flows from the gate current in its line

AFM image, investigate the variation of the induced voltage in a serial-channel SFFT as a function of the gate current by the I–V measurement system. We measured their transistor characteristics in order to confirm the operation of a serial-channel SFFT. We performed the numerical simulation to get the theoretical characteristics of a serial-channel SFFT controlled by a gate current via the modified channel. The experimental results are approximately in agreement with simulation ones.

2 Experimental

A scheme of an SFFT with a serial-channel type is shown in Fig. 1. The serial-channel SFFT is composed of a gate current line and drain current line with a weak-link. The magnetic field generated by the gate current controls the induced voltage across the weak-link or the serial-channel. The total width (w_t) of a drain current line was 40 μm. It contained serial channel no. 1 and no. 2 of drain current line that was 10 μm widths (w_1, w_2) and 5 μm lengths (L_1, L_2), respectively. The parallel length (w_b) between the external edge and the channel no. 1 or no. 2 edge of the drain current line was 15 μm. The vertical length (L_0) between channel no. 1 and channel no. 2 was 10 μm. The gate current line with 20 μm width (w_0) was located 5 μm (a_0) from the edge of the drain current line.

When the gate currents are applied to the gate current line, the magnetic flux density in the channel no. 1 and no. 2 are calculated using the Biot-Savart's law at the mean point of the drain current line as shown in Fig. 2. To analogy easily the final current–voltage characteristic equation induced at the channel terminals of the drain current line, the serial-channel no. 1 and no. 2 should be satisfied with equilibrium conditions. Channel length L_1 and L_2, channel width w_1 and w_2, and channel thickness d_1 and d_2 are equal to each other, respectively. As a result, the current–voltage characteristic equation induced at the channel terminals of the drain current line by the gate current (I_g) can be written as follows:

$$\begin{cases} V_{ds} = \left[\frac{4\mu_0(2L_1+L_0)k_BT\delta}{d_1 h}\exp^{-\left(E_p/k_BT\right)}\right][I_d - I_{crTs}] \times \sinh\left[\frac{I_d}{w_1 k_B T/\delta\phi_0}\right], & for\ I_d \geq I_{crTs}, \\ V_{ds} = 0, & for\ I_d < I_{crTs}. \end{cases} \quad (1)$$

Where k_B and δ are Boltzman's constant and pinning potential range, respectively. E_p and ϕ_0 are the pinning energy at temperature (T) and the flux quantum, respectively. μ_0 and ħ are the permeability of vacuum and the Planck's constant, respectively. I_{crTs} is the total critical current of a serial-channel SFFT in the drain current line. I_{cr0} is the initial critical current with no magnetic interaction generated by the gate current. The total critical current I_{crTs} is given by

$$I_{crTs} = \left[I_{cr0} - \frac{d_1 I_g}{k_s}\left(\frac{k_{sn1}}{w_g + w_b} - \frac{k_{sf1}}{w_g + w_b + w_1}\right)\right]. \quad (2)$$

Where the magnetic coupling coefficients are given by

$$k_{sn1} = \frac{\sin\alpha}{2\pi}\left\{\sin\left(\tan^{-1}\frac{x_0\tan\alpha+0.5L_0+0.5L_1}{w_g+w_b}\right)+\sin\left(\tan^{-1}\frac{x_0\tan\alpha-0.5L_0-0.5L_1}{w_g+w_b}\right)\right\}$$
$$k_{sf1} = \frac{\sin\alpha}{2\pi}\left\{\sin\left(\tan^{-1}\frac{x_0\tan\alpha+0.5L_0+0.5L_1}{w_g+w_b+w_1}\right)+\sin\left(\tan^{-1}\frac{x_0\tan\alpha-0.5L_0-0.5L_1}{w_g+w_b+w_1}\right)\right\}. \quad (3)$$

Where k_{sn1} and k_{sf1} are the magnetic coupling coefficients related to the channel width and the channel length between the channel no. 1 and no. 2 of the drain current line and the gate current line. k_s is the fitting parameter related to the gate current in a serial-channel SFFT after anodizing the serial-channel by an AFM lithography method. As the channel length increases, the output voltage increases from Eq. 1. As known in Eq. 2, the total critical current is varied

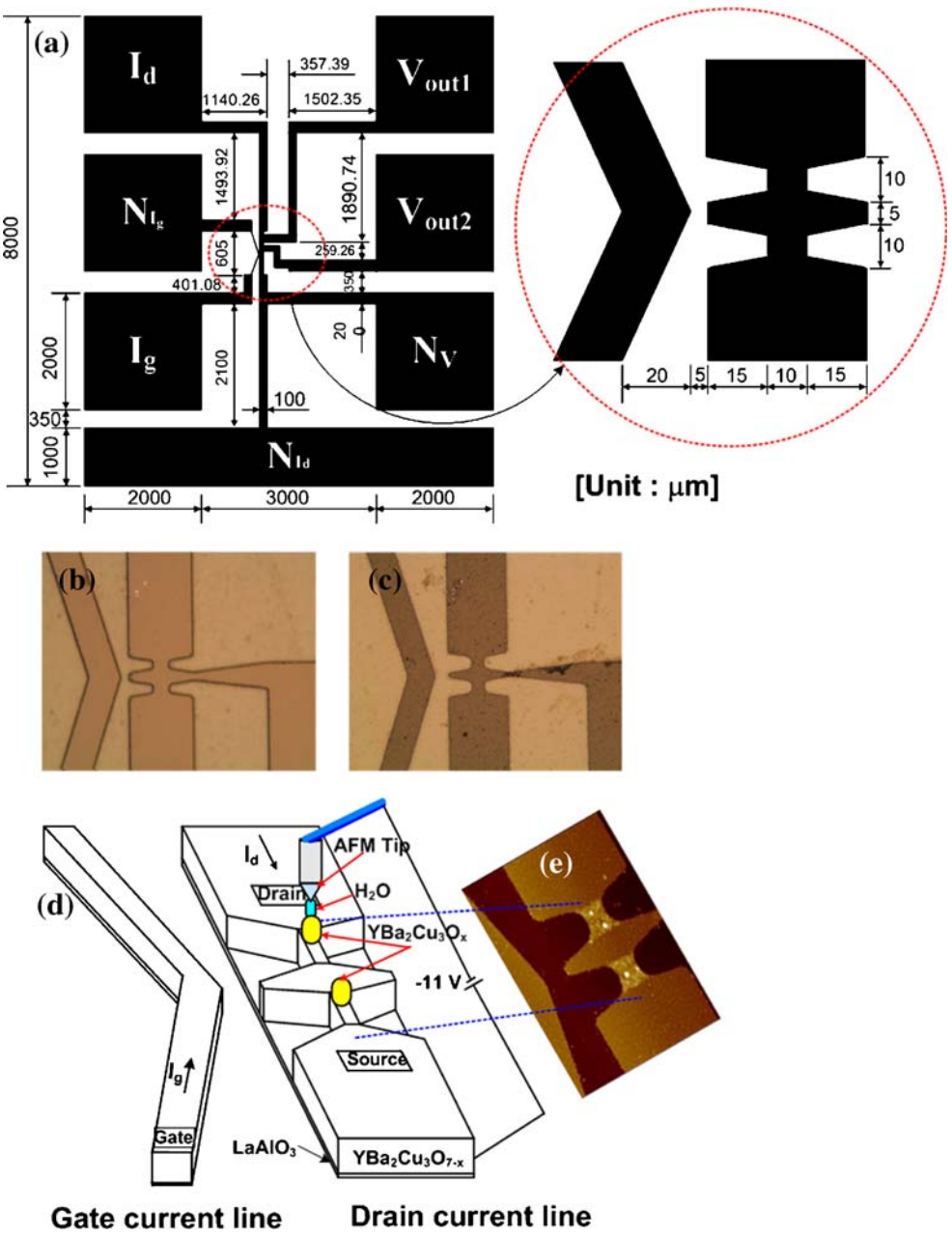

Fig. 3 The fabrication process of a serial-channel SFFT using an AFM lithography method. (**a**) The drawing of mask pattern. (**b**) The pattern developed by a photo lithography method. (**c**) The photo microscope image of a sample fabricated by a wet etching method. (**d**) The fabrication scheme by an AFM lithography and e the topography of a serial-channel SFFT fabricated by an AFM lithography method

according to the parameter related to the gate current, channel width, w_g, w_b, and the length of drain current line. When this critical current is same or larger than drain current, the output voltage are induced in the channel by the applied magnetic field, which is generated by the gate current.

In order to fabricate the SFFT with a serial-channel type, it is need to fabrication process as shown in Fig. 3. Superconducting YBCO thin film with approximately 360 nm thickness was prepared on a $LaAlO_3$ substrate by the thermal evaporation deposition method. The critical temperature (T_c) and current density (J_c) for S-type superconducting YBCO thin film were approximately 88.4 K and 2.0 MA/cm^2, respectively. The samples were patterned by a conventional etching method using photoresist and H_3PO_4 etchant in order to fabricate drain, source, and gate of an SFFT as shown in Fig. 3(a)–(d). Figure 3(a) presents the drawing of mask pattern. Figure 3(b) and (c) describe the pattern developed by a photo lithography method and the photo microscope image of a sample fabricated by a wet etching method using H_3PO_4 etchant. The middle between the drain and a source [see Fig. 3(d)] in a conventional SFFT was lithographed with an AFM system (Nanoscope IV Multimode, Digital Instruments Inc., USA) as a channel. Figure 3(e) presents the topography of a serial-channel after oxidizing by AFM bias voltage at −11 V. The serial channels with a 10 μm×5 μm were constructed by localized anodization using an AFM lithography method. The AFM was operated in a contact mode at force of 10.5 nN, under ambient condition with a relative humidity of over 50%. The serial-channel of the SFFT was modified using a TiO_x coating tip, which was biased to a negative voltage with respect to the channel surface, across the 32 μm×8 μm size of a serial-channel at a scan rate of 0.68 Hz and tip velocity of 43.4 μm/s.

3 Results and discussion

In order to investigate the current–voltage characteristics of a serial-channel SFFT fabricated by an AFM lithography method, we have analyzed the modified surface topography by an AFM tapping mode. An AFM image of a serial-channel SFFT fabricated by a wet chemical etching method is shown in Fig. 4(a).

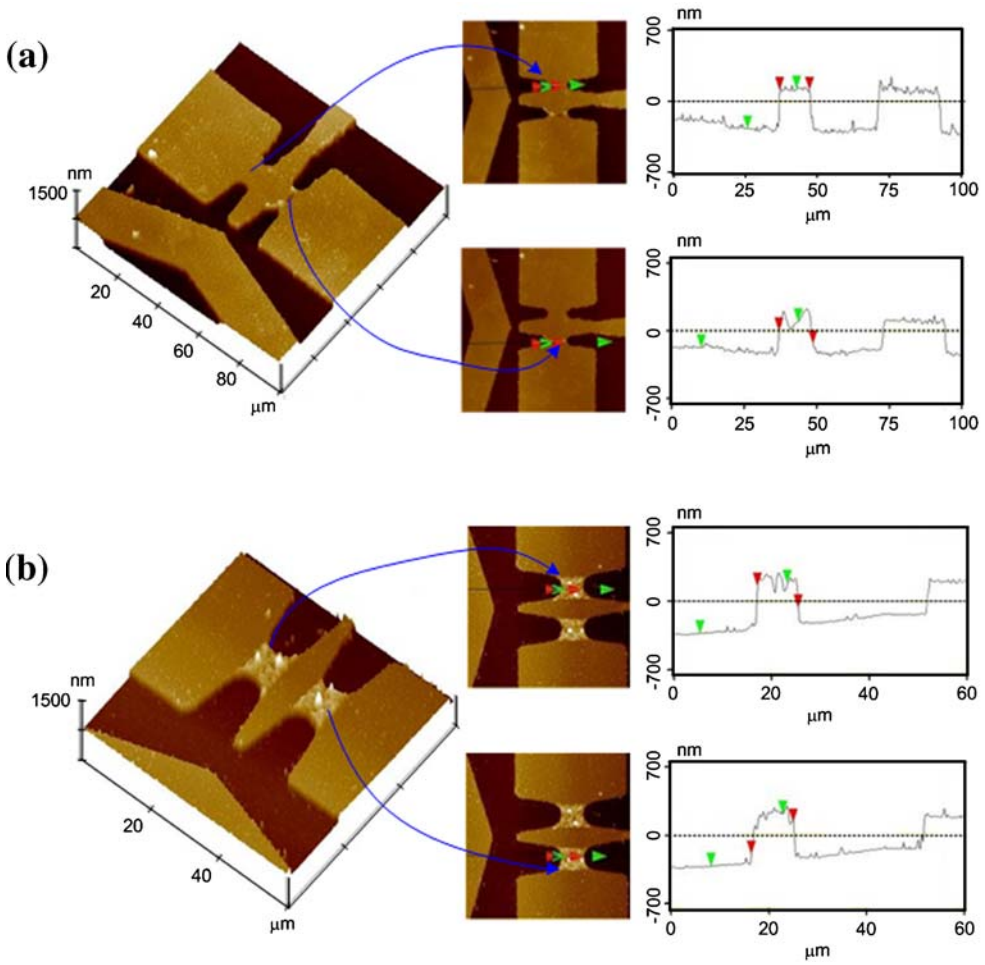

Fig. 4 Section analysis and AFM 3D image of the surface topography a before and b after AFM lithography in the serial-channel no. 1 and no. 2

Before AFM lithography, the heights of a serial-channel in the channel no. 1 and no. 2 are 303, 268 nm, respectively. Figure 4(b) shows the anodized serial-channel with 8.5, 10.5 μm widths and 508, 403 nm heights in the channel no. 1 and no. 2 after anodization by an AFM at −11 V tip bias, respectively. We have fabricated the SFFT with maximum protrusion distances approximately 205 and 135 nm in the serial-channel no. 1 and no. 2 using an AFM oxidation process, respectively.

The thickness variations of the channel effect on the critical current density of the SFFT with superconducting thin films. As the thickness of the channel is thick, the applied electric field due to the gate current is not sensitive for the channel, so the transresistance is small. In conventional studies [24], the thickness of the strips was increased with increasing the bias voltage or scanning number of AFM tip, indicating that it could produce the same effect by an increase of them. Also, the oxidized thickness of superconducting thin films is affected by various anodization conditions [25, 26].

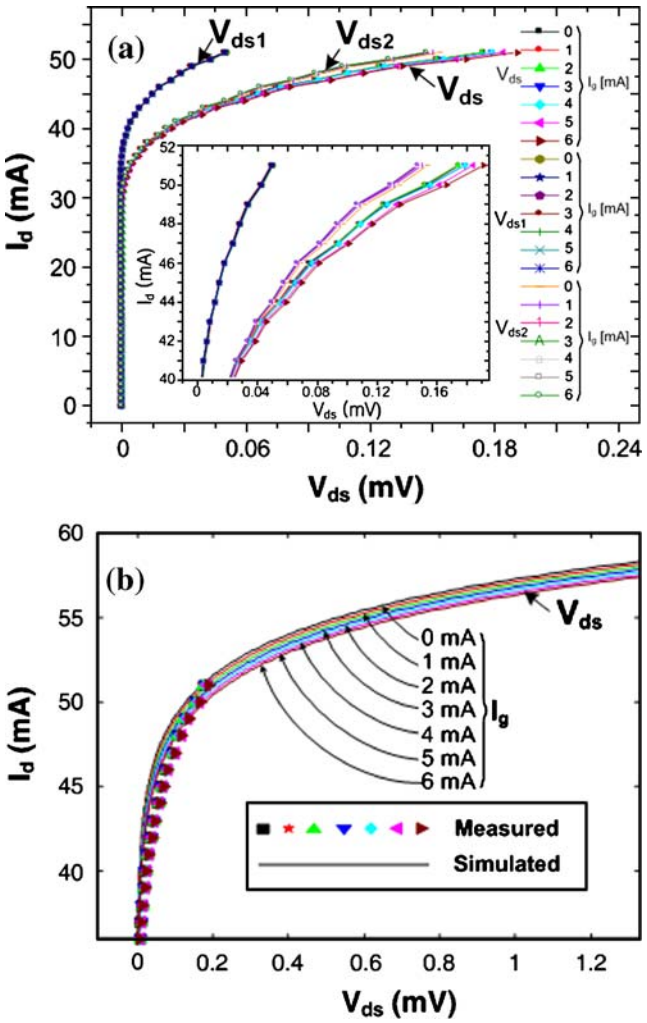

Fig. 5 Current–voltage characteristic curves of a serial-channel SFFT fabricated by an AFM lithography method. (**a**) Measured results between the terminals of channel no. 1 and no. 2, and (**b**) calculated results after AFM lithography

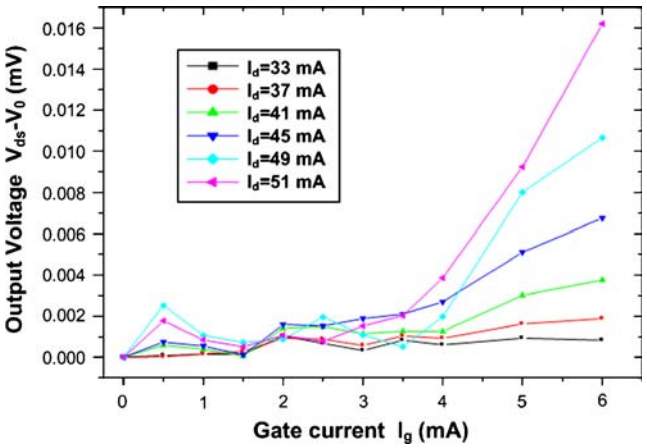

Fig. 6 Flux flow characteristics of a serial-channel SFFT

Figure 5(a) shows the current–voltage curves of a serial-channel modified with the negative bias voltage of −11 V. With no applying the gate current, the total critical current in the serial-channel was 32.7 mA and the critical currents in the channel no. 1 and no. 2 were 38.6, 32.5 mA, respectively. When the gate currents increase from 0 mA up to 6 mA at 1 mA steps in the gate terminal, the critical currents generated by a gate current decrease at narrow interval. The current–voltage characteristic curves simulated from Eq. 1 are plotted in Fig. 5(b), which are calculated from the data of the section analysis of the surface formed after AFM lithography in the serial-channel no. 1 and no. 2. The simulated curves are approximately corresponded to the measured ones.

Figure 6 describes the flux flow characteristics of a serial-channel SFFT. In order to calculate the induced voltages by an externally applied magnetic field, the self-induced voltage V_0 is subtracted from the flux flow voltage V_{ds}. The flux flow characteristics can be obtained by replotting V_{ds}–V_0 vs

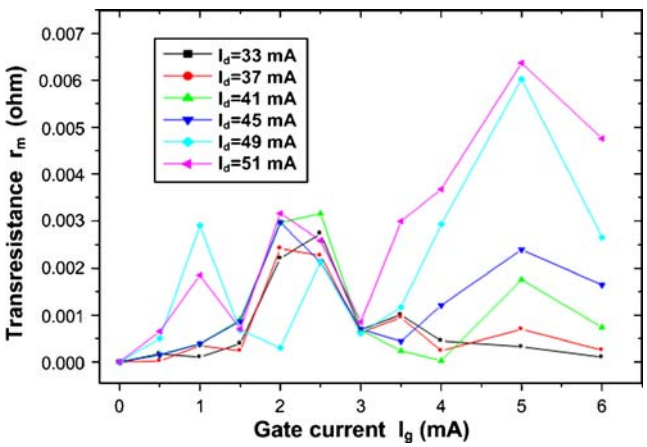

Fig. 7 Gate current dependence of the transresistance calculated from the flux flow characteristics of a serial-channel SFFT

I_g for constant I_d. The slope of the output voltage decreased at I_g=5 mA as shown in Fig. 6. The reason can be explained as follows. In a device without channel modification such as etching or anodization, the vortices flow out from the channel at a high gate current level because the film thickness of the channel is equal to that of the drain current electrode film. By contrast, in a device with a modified channel, the vortices cannot overflow from the channel even at a high gate current level owing to the barrier in a modified channel by AFM lithography. In a device with a transformed channel, it is expected that higher energy will be required to enable the vortices to flow out of the channel and enter the electrode films.

From the data of the flux flow characteristics using $r_m = \Delta V_{ds}/\Delta I_g$, we can calculate the transresistance r_m which are the parameters to present the characteristics of a serial-channel SFFT. The transresistance r_m vs I_g is plotted in Fig. 7. The transresistance decreased rapidly for gate current values higher than 5 mA in the SFFT with a serial-channel type as shown in Fig. 7. The peak value of the transresistance was about 0.006 Ω for I_d=51 mA at I_g= 5 mA. The transresistance values were extremely fluctuated below I_g=3 mA. It is considered due to unequilibrium relationship between channel no. 1 and channel no. 2 after AFM lithography. The oxidized channel regions will act as a pinning center during the operation of a serial-channel SFFT, which can be cause of a low transresistance value.

4 Conclusion

We have used AFM lithography in combination with an improved aqueous etch to fabricate a serial-channel SFFT with dimensions on the order of 5 μm. The devices operate at 77 K and have characteristics in agreement with results expected from the numerical simulation. The maximum transresistance value was about 0.006 Ω for I_d=51 mA at I_g=5 mA. Though it did not show a high transresistance in comparison with SFFTs fabricated by the other lithography processes, our results indicate that the serial-channel having an effect as a weak link is effectively fabricated by an AFM lithography method instead of fabrication weak link using an Ar ion milling or inductively coupled plasma. In future, the YBCO oxidization properties produced by AMF anodization will be studied for the various channels SFFTs. Expressly, the thickness section analysis of the modified channel will be performed by the Nanofinder and AFM tapping mode.

References

1. J.A. Dagata, J. Schneir, H.H. Harary, C.J. Evans, M.T. Postek, J. Bennett, Appl. Phys. Lett. **56**(20), 2001 (1990)
2. H.C. Day, D.R. Allee, Appl. Phys. Lett. **62**(21), 2691 (1993)
3. E.S. Snow, P.M. Campbell, Appl. Phys. Lett. **64**(15), 1932 (1994)
4. T. Teuschler, K. Mahr, S. Miyazaki, M. Hundhausen, L. Ley, Appl. Phys. Lett. **67**(21), 3144 (1995)
5. F. Pérez-Murano, G. Abadal, N. Barniol, X. Aymerich, J. Servat, P. Gorostiza, F. Sanz, J. Appl. Phys. **78**(11), 6797 (1995)
6. J. Servat, P. Gorostiza, F. Sanz, F. Pérez-Murano, N. Barniol, G. Abadal, X. Aymerich, J. Vac. Sci. Technol. A. **14**, 1 (1996)
7. T. Sumomogi, T. Endo, K. Kuwahara, R. Kaneko, T. Miyamoto, J. Vac. Sci. Technol. B. **12**, 1876 (1994)
8. X. Jin, W.N. Unertl, Appl. Phys. Lett. **61**(6), 657 (1992)
9. S. Hu, A. Hamidi, S. Altmeyer, T. Köster, B. Spangenberg, H. Kurz, J. Vac. Sci. Technol. B. **16**, 2822 (1998)
10. R. Magno, B.R. Bennett, Appl. Phys. Lett. **70**(14), 1855 (1997)
11. H.W. Schumacher, U.F. Keyser, U. Zeiter, R.J. Haug, Appl. Phys. Lett. **75**(8), 1107 (1999)
12. M. Faucher, T. Fournier, B. Pannetier, C. Thirion, W. Wernsdorfer, J.C. Villegier, V. Bouchiat, Physica C. **368**, 211 (2002)
13. S.C. Minne, H.T. Soh, P. Flueckinger, C.F. Quate, Appl. Phys. Lett. **66**(6), 703 (1995)
14. P.M. Campbell, E.S. Snow, P.J. Mcmarr, Appl. Phys. Lett. **66**(11), 1388 (1995)
15. M. Nakamura, H. Yanagisawa, S. Kuratani, M. Iizuka, K. Kudo, Thin Solid Films. **438–439**, 360 (2003)
16. T. Banno, M. Tachiki, H. Seo, H. Umezawa, H. Kawarada, Diam. Relat. Mater. **11**, 387 (2002)
17. I.S. Song, B.M. Kim, G.S. Park, Appl. Phys. Lett. **76**(5), 601 (2000)
18. T. Schmidt, R. Martel, R. Sandstrom, P. Avouris, Appl. Phys. Lett. **73**(15), 2173 (1998)
19. J.S. Martens, G.K.G. Hohenwarter, J.B. Beyer, J.E. Nordman, D.S. Ginley, J. Appl. Phys. **65**(10), 4057 (1989)
20. J.S. Martens, V.M. Hietala, T.E. Zipperian, D.S. Ginley, C.P. Tigges, J.M. Phillips, IEEE Trans. Microwave Theor Tech. **39** (12), 2018 (1991)
21. K. Miyahara, K. Tsuru, S. Kubo, M. Suzuki, IEEE Trans. Appl. Supercond. **5**(2), 3381 (1995)
22. H.G. Kang, Y.H. Lim, S. Ko, S.H. Lim, B.S. Han, Y.B. Hahn, Physica C. **400**(3–4), 111 (2004)
23. K. Miyahara, S. Kubo, M. Suzuki, J. Appl. Phys. **76**(8), 4772 (1994)
24. H.G. Kang, S. Ko, K.Y. Jahng, H. Lee, Phys. Stat. Sol. (c). **2**(5), 2173 (2005)
25. H.G. Kang, S.K. Kim, H. Lee, Surf. Sci. **600**(18), 3673 (2006)
26. H.G. Kang, J.B. Park, K.Y. Jahng, H. Lee, JPN. J. Appl. Phys. **45** (3B), 2361 (2006)